

GA-A23029

**ADVANCED TOKAMAK PHYSICS
EXPERIMENTS ON DIII-D**

by
T.S. TAYLOR and THE DIII-D TEAM

DECEMBER 1998

DISCLAIMER

This report was prepared as an account of work sponsored by an agency of the United States Government. Neither the United States Government nor any agency thereof, nor any of their employees, makes any warranty, express or implied, or assumes any legal liability or responsibility for the accuracy, completeness, or usefulness of any information, apparatus, product, or process disclosed, or represents that its use would not infringe privately owned rights. Reference herein to any specific commercial product, process, or service by trade name, trademark, manufacturer, or otherwise, does not necessarily constitute or imply its endorsement, recommendation, or favoring by the United States Government or any agency thereof. The views and opinions of authors expressed herein do not necessarily state or reflect those of the United States Government or any agency thereof.

GA-A23029

**ADVANCED TOKAMAK PHYSICS
EXPERIMENTS ON DIII-D**

by
T.S. TAYLOR and THE DIII-D TEAM

This is a preprint of an invited paper presented at the Japanese Physical Society Meeting, December 1-4, 1998, Yokohama, Japan and to be published in *The Proceedings*.

Work supported by
the U.S. Department of Energy under
Contract Nos. DE-AC03-99ER54463, DE-AC05-96OR22464,
W-7405-ENG-48, DE-AC02-76CHO3073, and
Grant No. DE-FG03-96ER54373

**GA PROJECT 3466
DECEMBER 1998**

ABSTRACT

Significant reductions in the size and cost of a fusion power plant core can be realized if simultaneous improvements in the energy confinement time (τ_E) and the plasma pressure (or beta $\beta_T = 2 \mu_0 \langle p \rangle / B_T^2$) can be achieved in steady-state conditions with high self driven bootstrap current fraction. In addition, effective power exhaust and impurity and particle control is required. Significant progress has been made in experimentally achieving regimes having the required performance in all of these aspects as well as in developing a theoretical understanding of the underlying physics. We have extended the duration of high performance ELMing H-mode plasmas with $\beta_N H_{89p} \sim 10$ for $5 \tau_E$ (~ 1 s) and have demonstrated that core transport barriers can be sustained for the entire 5-s neutral beam duration in L-mode plasmas. Recent DIII-D work has advanced the understanding of improved confinement and internal transport barriers in terms of E×B shear stabilization of micro turbulence. With the aim of current profile control in discharges with negative central magnetic shear, we have demonstrated off-axis electron cyclotron current drive for the first time in a tokamak, finding an efficiency above theoretical expectations. MHD stability has been improved through shape optimization, wall stabilization, and modification of the pressure and current density profiles. Heat flux reduction and improved impurity and particle control have been realized through edge/divertor radiation and understanding and utilization of forced scrape off layer flow and divertor baffling.

I. INTRODUCTION

The viability of a tokamak as an economically and environmentally attractive power plant requires for ignition margin, sufficient energy confinement time (τ_E), for adequate fusion power density, sufficient volume average toroidal beta, $\beta = 2 \mu_0 \langle P \rangle / B^2$, and for low steady-state recirculating power, sufficient self-driven bootstrap fraction. An energy confinement enhancement, $H_{89P} \equiv \tau_E / \tau_{E \text{ ITER89P}} \gtrsim 2$, or $H_{98Y} \equiv \tau_E / \tau_{E \text{ ITER98Y}} \approx 1$, and a normalized beta, $\beta_N \equiv \beta / (I/aB) \geq 2.5\% \text{-m-T/MA}$, are considered sufficient for ignition, and engineering testing in ITER.¹ $\tau_{E \text{ ITER89P}}$ is the ITER L-mode energy confinement scaling,² and $\tau_{E \text{ ITER98Y}}$ is the thermal energy confinement scaling for ELMing H-mode.¹ A number of short pulse tokamak experiments have obtained confinement with $H_{89P} \sim 3\text{--}4$, and high normalized beta, $\beta_N \sim 4\text{--}6$, have been observed in some cases.³ If this factor of near two improvements in performance can be maintained in steady-state conditions, an approximate factor of two reduction in size, capital cost, and cost of electricity for a fusion power plant could be gained.^{4,5}

The DIII-D research program is aimed at developing the scientific basis for advanced modes of operation which can enhance the commercial attractiveness of the tokamak as an energy producing system. Features that improve the attractiveness of the tokamak as a fusion power plant are those mentioned above, high β , high τ_E , and high bootstrap fraction, as well as adequate divertor heat removal, particle and impurity control. The study of tokamak operational scenarios which simultaneously achieve these features has become known as "advanced tokamak" (AT) research.

This manuscript is a report of progress in the AT research in DIII-D. In Section II, we report on the progress toward increasing the duration of high performance discharges on DIII-D, and NCS discharges as a steady-state scenario. In Section III, we discuss the progress in understanding the transport and transport barriers in DIII-D, and initial results of off-axis current drive with electron cyclotron current drive (ECCD). Our present understanding and progress in stability are given in Section IV, including the effects of the pressure profile, neoclassical tearing modes, and wall stabilization. In Section V, we report progress in high density discharges, the impact of flows on impurity enrichment and the understanding of convection and recombination in radiative divertor plasmas. In Section VI is a short summary.

II. PROGRESS TOWARDS INTEGRATED, STEADY-STATE, IMPROVED PERFORMANCE PLASMAS

In order to establish their future relevance for fusion, improved performance scenarios must demonstrate a path towards ultimate steady-state operation. This requires demonstrating that improved confinement plasmas can be sustained for long pulses at high beta values as well as developing the tools which will be needed for steady state operation.

Figure 1 demonstrates our progress during 1998 in moving towards steady-state improved performance discharges. In this figure, we measure our approach to steady state with $\tau_{\text{duration}}/\tau_E$, the duration of the high confinement phase divided by the energy confinement time. We measure advanced tokamak performance through the product of normalized beta, $\beta_N = \beta (aB_T/I_p)$, and the confinement enhancement factor H relative to the ITER confinement scaling law. For ELMing H-mode, we will use H_{98y} , which is defined relative to the most recent scaling for thermal energy confinement time in ELMing H-mode.¹ An example of such an improved performance discharge is shown in Fig. 2.⁶ Lines indicating the β_N and H_{98y} values required for ITER and the ARIES-RS reactor study⁵ are also shown, indicating that this discharge exceeds the ARIES-RS requirements on the $\beta_N H_{98y}$ product. A $\beta_N H_{98y}$ product exceeding 6 is sustained for 1 s ($5 \tau_E$).

Two approaches have been taken to improve plasma performance and duration as is illustrated in Fig. 3. One approach is more aggressive in pushing high power to reach high β_N while the second has emphasized more the long pulse aspects. Both utilize the technique of an early neutral beam injection during the current ramp that was developed over the past several years in developing the negative central shear scenario and producing core transport barriers in DIII-D,^{7,8} JET,⁹ JT60-U,¹⁰ and TFTR.^{11,12} A key feature in sustaining the good performance in these discharges is the absence of sawteeth and $q(0) \gtrsim 1$. Neither shot shows the rapid, localized change in temperature gradient characteristic of a strong, localized core transport barrier; however, transport analysis indicates improvement in ion thermal diffusivity over most of the discharge relative to standard ELMing H-mode.

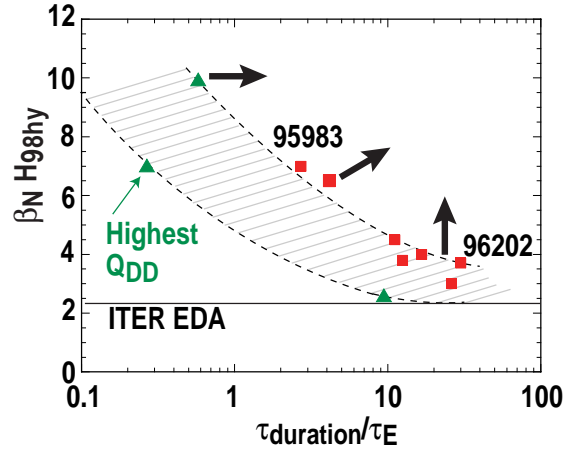


Fig. 1. Plot of the $\beta_N H_{98y}$ product versus normalized discharge duration for DIII-D prior to 1998 (triangles) and more recent shots (squares). The shaded region shows our progress during 1998. All these discharges are H-modes; accordingly, the confinement enhancement factor H_{98y} relative to the H-mode scaling is used.

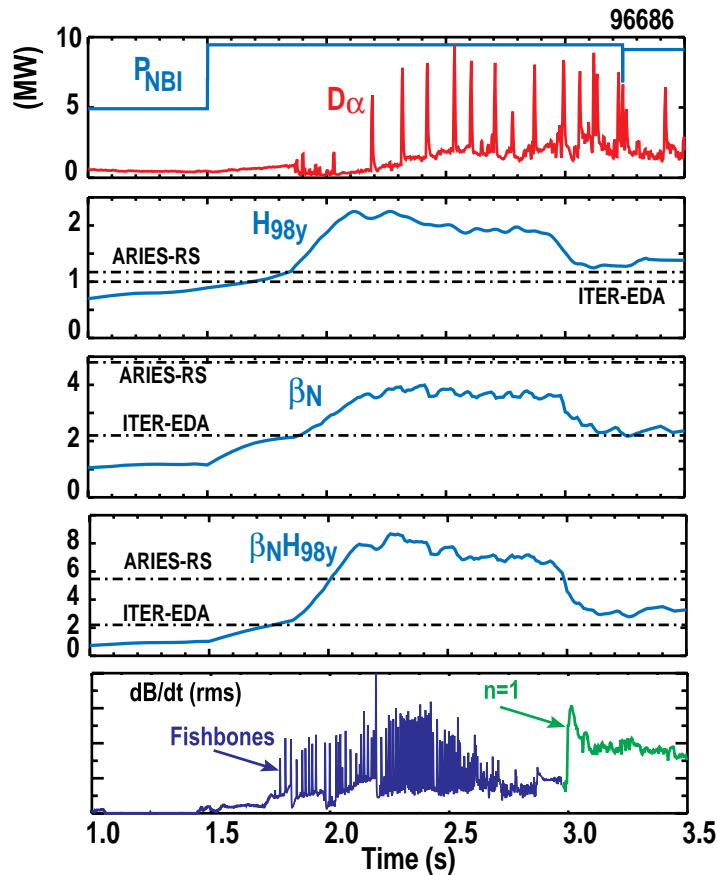


Fig. 2. Time evolution of a high performance DIII-D discharge. The 1 s duration is comparable to the current profile relaxation time scale. Some parameters of interest during the high performance phase are: $\beta \sim 4.5\%$, $n_e/n_{Gr} \sim 0.5$, $q(0) \sim 1$, $q_{95} = 4.4$, $\tau_{th} \sim 0.21$ s, and $f_{bs} \sim 50\%$, where n_{Gr} is the Greenwald density and f_{bs} is the bootstrap fraction.

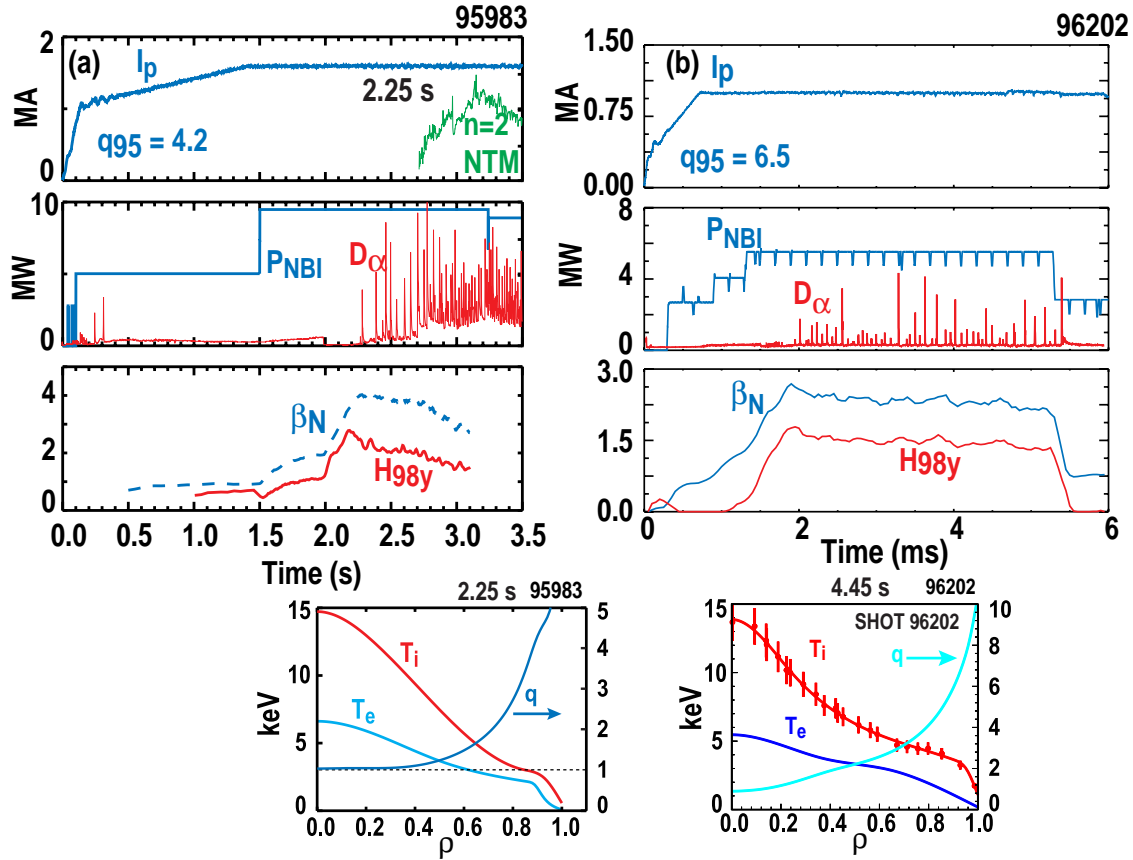


Fig. 3. Time histories and radial profiles of two recent DIII-D shots emphasizing long pulse high performance. Shot 95983 (a) reached $\beta_N H_{98y}$ about 7 for $3 \tau_E$ while 96202(b) achieved $\beta_N H_{98y}$ around 3 for $25 \tau_E$. (The corresponding $\beta_N H$ products using the ITER89P L-mode scaling are 10 and 5 respectively.) The high performance phase of shot 96202 was terminated only when the neutral beam power was turned down while that of 95983 degraded due to the onset of neoclassical tearing modes. Shot 95983 was at 2.1 T toroidal field and had a line averaged density $5.4 \times 10^{19} \text{ m}^{-3}$ during the high performance phase while shot 96202 was at 1.9 T toroidal field and had a line averaged density of $2.7 \times 10^{19} \text{ m}^{-3}$.

High performance is obtained in these discharges with modest bootstrap current: the bootstrap fraction is approximately 50%. Alignment of the bootstrap current at high bootstrap fraction requires a slight modification of the current profile to a hollow current profile and a region of negative magnetic shear.^{13–16} This regime has been obtained experimentally on many tokamaks, and highest performance in DIII-D¹⁷ and JT-60U¹⁸ has been transiently obtained in the negative central magnetic shear (NCS) scenario. There are a number of advantages to the NCS scenario including, bootstrap alignment at high bootstrap fraction, the potential for high beta with wall stabilization, and proven high confinement with an internal transport barrier (ITB). The challenge remains to develop transport understanding, transport barrier control and current profile control to extend the NCS regime to steady state.

III. UNDERSTANDING AND CONTROLLING CORE TRANSPORT

In order to extend the improved performance results from present machines to future devices with confidence, we must finally develop a predictive understanding of tokamak transport and transport barriers. In addition, improved performance scenarios, especially in self-heated burning plasmas, will require development of new tools to control transport.

In the NCS regime, an ITB is often observed in the ion thermal and particle transport, and sometimes in the electron thermal transport. The ITB is observed as a rapid change in the gradient of the ion temperature, and the rotation velocity on DIII-D.¹⁹ In NCS discharges with an H-mode edge, the ion transport is observed to be near the neoclassical level across the entire discharge. Although, an ITB is often observed in the ion channel in discharges with weak positive magnetic shear, the ITB is most clearly reproducibly obtained with negative shear. An ITB in the electron thermal channel is only observed with negative magnetic shear. A comparison of the transport of two discharges, one with weak positive shear, and a second with negative magnetic shear is shown in Fig. 4. In Fig. 4(a), the ion transport is near the neoclassical level across the entire discharge, and the electron transport is not much changed (it is reduced near the boundary as in most H-mode discharges). In Fig. 4(b), a discharge with large negative shear in the core, exhibits a clear reduction in both the ion and electron transport channel.²⁰

The reduction of transport is consistent with sheared $E \times B$ flow stabilization of microturbulence.¹⁹⁻²² Elevated $q(0)$ and the negative magnetic shear stabilizes MHD turbulence. Sheared $E \times B$ flow decorrelates the turbulent eddies, reducing transport. Complete stabilization is predicted when the measured $E \times B$ shearing rate, $\omega_{E \times B}$, exceeds the calculated maximum linear growth rate, γ_{\max} . The measured reduction in transport; the measured reduction in density fluctuations from far infrared scattering, beam emission spectrometry, and reflectometry; and the condition $\omega_{E \times B} > \gamma_{\max}$ are well correlated in space and time.

Although the creation of ion thermal and angular momentum transport barriers has been connected with $E \times B$ shear stabilization of turbulence both theoretically and experimentally, the physics governing the electron channel is less well understood. Electron thermal transport barriers are much more difficult to form in DIII-D than ion barriers and seem to require much greater magnetic shear.^{20,23,24} Electron heating with

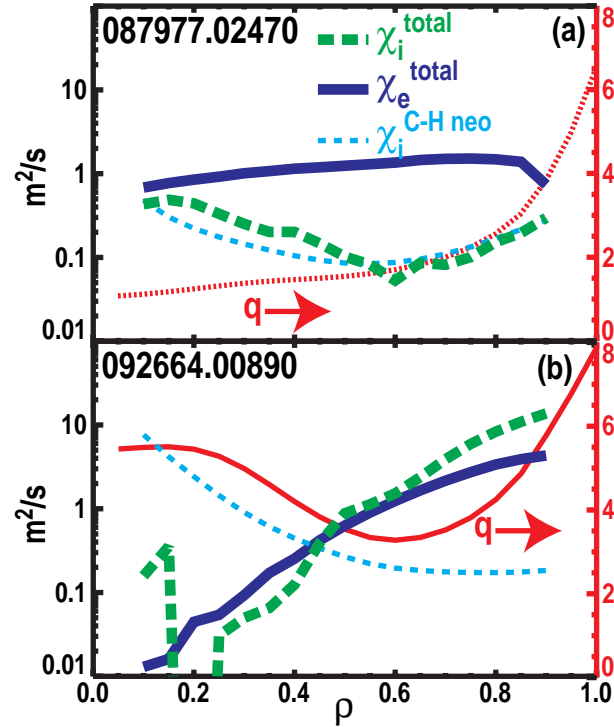


Fig. 4. Calculated thermal diffusivities from measured profiles from (a) a weak positive shear discharge with an H-mode boundary, and (b) an L-mode NCS discharge. χ_e , solid; χ_i , dashed, and $\chi_{i(\text{neo})}$, dotted.

either ECH or fast waves has been used to probe the physics of core transport barriers.^{24,25} For reasons that are not completely clear, central electron heating during the end of the core ion barrier formation phase tends to weaken the ion barrier, resulting in some reduction in core ion temperature and core ion rotation. This effect occurs only within the core barrier region with the ion profiles outside this region remaining unchanged by the additional electron heating. Both ion and electron thermal diffusivities increase after the application of the core electron heating, with the electron diffusivity rising almost an order of magnitude.^{20,24} The changes in the ion channel in these discharges are consistent with change in the $E \times B$ shearing rate relative to the low k turbulence growth rates.^{20,24} The decreased ion rotation gives a decreased $E \times B$ shear while the growth rate changes little. However, the physics of the electron channel in these plasmas remains unexplained.^{20,24} Recent FIR scattering measurements of short wavelength turbulence at $k = 12 \text{ cm}^{-1}$ have shown measurable turbulence whose onset is correlated with the start of the electron heating, which suggests high k turbulence may be affecting electron transport.

The core transport barriers can be sustained for long durations. In modest current, and relatively low density of $2 \times 10^{19} \text{ m}^{-3}$, L-mode edge discharges; core ion transport barriers have been run for the full 5 second neutral beam duration as shown in Fig. 5.

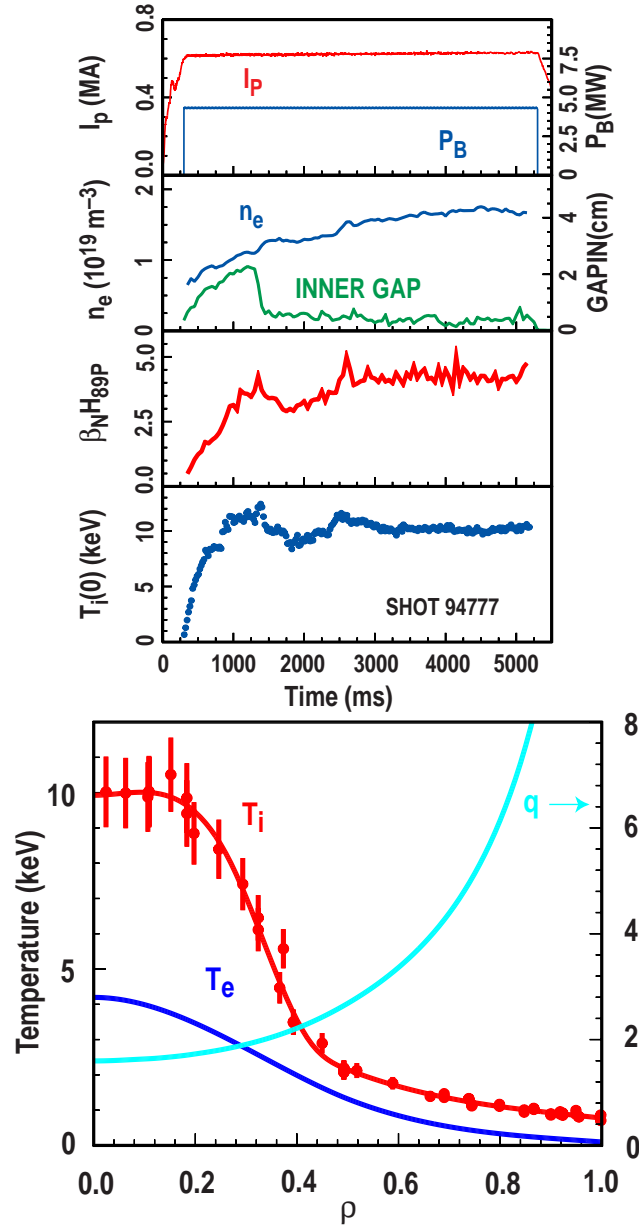


Fig. 5. Long pulse, L-mode edge discharge 94777 run at 1.9 T toroidal field; (a) temporal evolution of discharge parameters, (b) profiles shown at 4500 ms. Discharge including q profile is essentially reached steady state at 4500 ms, $q(0) = 1.6$.

The transport barrier formed early in the discharge, $t = 0.7$ s, when $q(0) \sim 3.5$, and the q profile was quite flat near the core. Before the end of the discharge the current profile is fully penetrated [Fig. 5(a)] and is no longer evolving, with $q(0) \sim 1.6$. As seen in Fig. 5, parameters such as $T_i(0)$, N_e , and β_{NH89P} are nearly stationary for the last 2 seconds of the discharge. Such a discharge demonstrates that it is possible to create an ion transport barrier which can last indefinitely. The core transport barriers with such long duration are so far obtained at modest current. A necessary condition for maintaining the transport

barrier is keeping $q(0)$ above 1.0, preventing destruction of the core transport barriers by sawteeth and removing this trigger of neoclassical tearing modes. To keep $q(0)$ above one and maintain a weak shear or negative central shear discharge requires off axis current drive.

Because of the need for current profile control for advanced tokamak operation, investigation of electron cyclotron current drive (ECCD) is a key portion of the DIII-D research. In the past year, we have demonstrated off-axis ECCD on DIII-D for the first time in any tokamak.²⁶ Electron cyclotron wave power at 110 GHz, which is resonant near the second harmonic of the electron cyclotron resonance, can be steered over a range of minor radii by tilting the launching mirror in the poloidal direction. The waves are launched with a toroidal angle so they interact with electrons traveling in a preferred toroidal direction, generating toroidal current. Analysis was carried out using motional Stark effect measurements of the internal magnetic field, allowing the local driven current density to be determined.²⁷ A 4-point vertical scan of the deposition location was made, covering the range of 0.1 to 0.5 in normalized minor radius ρ . Figure 6(a) shows the profile of ECCD which is driven at a normalized radius of $\rho = 0.5$ by 1 MW of electron cyclotron power. The integrated net current driven is 35 kA. The gross behavior of the plasma — the evolution of the internal inductance, the time duration before the entry of the $q=1$ surface into the plasma as signified by the start of sawteeth — is consistent with the effects expected from the measured current drive for the different locations of the power deposition. The magnitude of the driven current exceeds the value calculated by linear (TORAY) or quasi-linear (CQL3D) codes. As is shown in Fig. 6(b), the theoretically predicted fall off in normalized efficiency with minor radius is not observed; the normalized efficiency at $\rho = 0.1$ and $\rho = 0.5$ are about the same. This result suggests that trapping of the heated electrons is much weaker than theoretically expected under the experimental conditions. These results strongly support the use of higher power ECCD as a means of sustaining current profiles with the optimized magnetic shear needed for advanced tokamak plasmas.

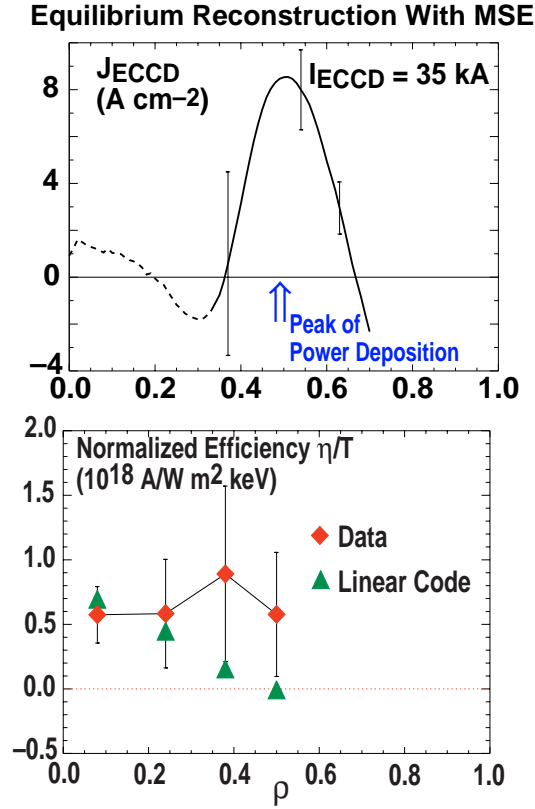


Fig. 6. (a) Profile of current density driven by ECCD for a case with power deposition at about half of the minor radius. (b) Normalized efficiency for ECCD as a function of the minor radius coordinate ρ . The experimental (diamonds) current drive efficiency η has been normalized by the local electron temperature to remove the theoretically expected temperature dependence. The experimental results are compared to the linear TORAY calculations (triangles) and show little decrease in normalized efficiency with ρ , contrary to theoretical expectations.

IV. PLASMA STABILITY

The key to steady state high performance is increasing stability limit at high beta, specifically, operation at high normalized beta is required. High power density, requires operation at high toroidal beta, and high bootstrap fraction requires operation at high poloidal beta, β_P . Steady state high performance requires both high power density and high bootstrap fraction, or since $\beta_P \times \beta_T \propto \beta_N^2$, high normalized beta is needed. Also, the steady-state energy gain depends very strongly on β_N ; $Q_{SS} = P_{FUS}/P_{CD} \propto \beta_N^2/q_{95}/(1 - \xi A^{1/2}q_{95}\beta_N)$, where ξ is profile dependent factor of the order of 0.02, and A is the aspect ratio. Note that ξ significantly increases for NCS q profiles compared to monotonic q profiles.

There are number of important methods for increasing β_N on DIII-D. These include strong plasma shaping, relatively broad pressure profiles, avoidance or stabilization of neoclassical tearing modes, and wall stabilization. The strong shaping, broad pressure profiles, and wall stabilization are synergistic effects, and these three effects taken together are needed for high beta in AT plasmas.²⁸

The dependence of the stability limit on peaking of the pressure profile for DIII-D shaped discharges ($\kappa \sim 1.8$, $\delta \sim 0.7$) is shown in Fig. 7. The stability boundaries are calculated for hollow current density profiles, and as shown the resistive interchange mode limit is typically 10%–20% below the ideal limit.^{28,29} In DIII-D discharges with peaked pressure profiles, modes that are identified as resistive interchange and ideal modes are both observed.²⁹ Note that the dashed curve for the L-mode NCS reaches a stability limit and β_N slightly greater than. In Fig. 7(b,c), the effect of broadening the pressure profile by programming an L- to H-mode transition is shown. At the L-H transition, the pressure profile broadens, and the discharge can continue stably to higher values of beta. Approximately a factor of 2 increase in β_N is obtained by broadening the pressure profile, in otherwise similar discharges, and $\beta_N > 4$ is obtained.

In long pulse H-mode discharges, modes identified as neoclassical tearing modes limit the duration of high performance. As is shown in Fig. 3(a), the performance in shot 95983 is degraded after 2.7 seconds by the onset of neoclassical tearing modes. This problem with neoclassical tearing modes is a common feature of many high performance discharges.⁸ These modes are metastable, requiring a finite-size magnetic island to trigger further growth. Finite-sized, seed islands can be triggered transiently, for example, by other MHD instabilities in the plasma, (e.g. sawteeth, ELMs or fishbones). As is shown in Fig. 8, the absence of sawteeth in shots like those in Fig. 3 removes one of the possible

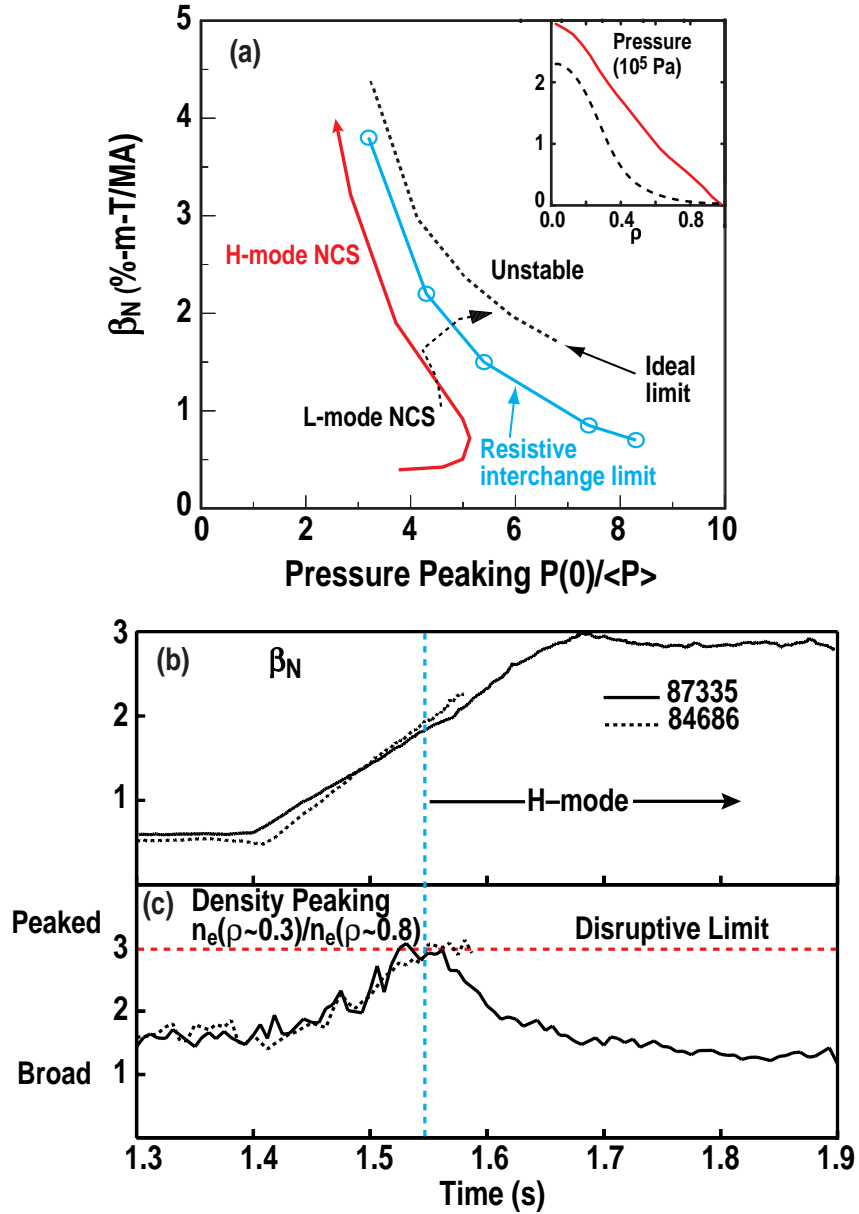


Fig. 7. Dependence of beta limit on pressure profile peaking; (a) β_N vs. $P(0)/\langle P \rangle$, dashed trace is the evolution of an L-mode NCS discharge in this parameter space, and the solid trace is the evolution of an H-mode NCS; (b) normalized beta, and (c) density peaking. In (b) and (c) the dotted trace is an L-mode NCS and discharge represented by the solid trace begins the same as the L-mode NCS, but makes a transition to H-mode at the indicated time.

sources of seed islands for the neoclassical tearing mode and thus allows operation at a higher beta value.³⁰ Negative magnetic shear is stabilizing to these modes. An attractive feature of the NCS discharges is the avoidance of these modes by negative shear, eliminating low order rational surfaces, and by eliminating the seed for the island, such as sawteeth.

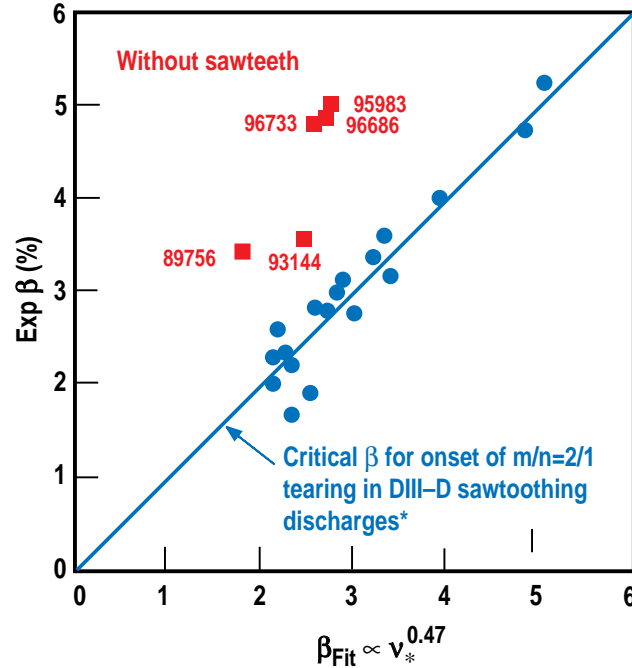


Fig. 8. The measured beta value for discharges similar to those in Fig. 2 (squares) significantly exceeds the neoclassical tearing mode limit established for sawtoothed discharges. The horizontal axis is the scaling value established in Ref. 30 while the line through the circular points is the best fit to the data for sawtoothed discharges. These neoclassical tearing modes are a mix of $m/n = 3/2$ and $2/1$ cases.

Equilibria with broad pressure profiles, broad current profiles and strong shaping, such as have been developed as NCS target equilibria, are strongly coupled to the plasma wall. Ideal stability calculations indicate that $\beta_N \sim 3\text{--}3.5$ with no wall stabilization, could be increased to $\beta_N > 5$ with a conducting wall at $r_w/a = 1.5$.²⁸ However, with a finite conducting wall, the resistive wall mode (RWM) is predicted to be unstable. We are evaluating the stabilization of the RWM by two techniques, plasma rotation, and active stabilization with external $n=1$ feedback coils.

We have developed a double current ramp technique to reliably and reproducibly make plasmas where the β_N values achieved indicates that wall stabilization of MHD modes is important.^{31,32} In addition, improved diagnostics have allowed us to make a direct identification of the resistive wall mode (RWM) mode structure in the plasma interior using ECE spectroscopy. Using these shots, we have achieved a new physics understanding of wall stabilization. We have produced rotating, wall stabilized discharges with the ratio of β_N to the no wall β_N limit (E_w) $\geq 1.4 \pm 0.05$. For example, in shot 92544, E_w exceeds unity for 200 ms, which is $>30 \tau_w$ (Fig. 9). The time constant τ_w is the $n = 1$ time constant of the wall ~ 5.8 ms. The plasma rotation slows as the beta increases beyond the no wall limit, and the RWM becomes unstable when the rotation

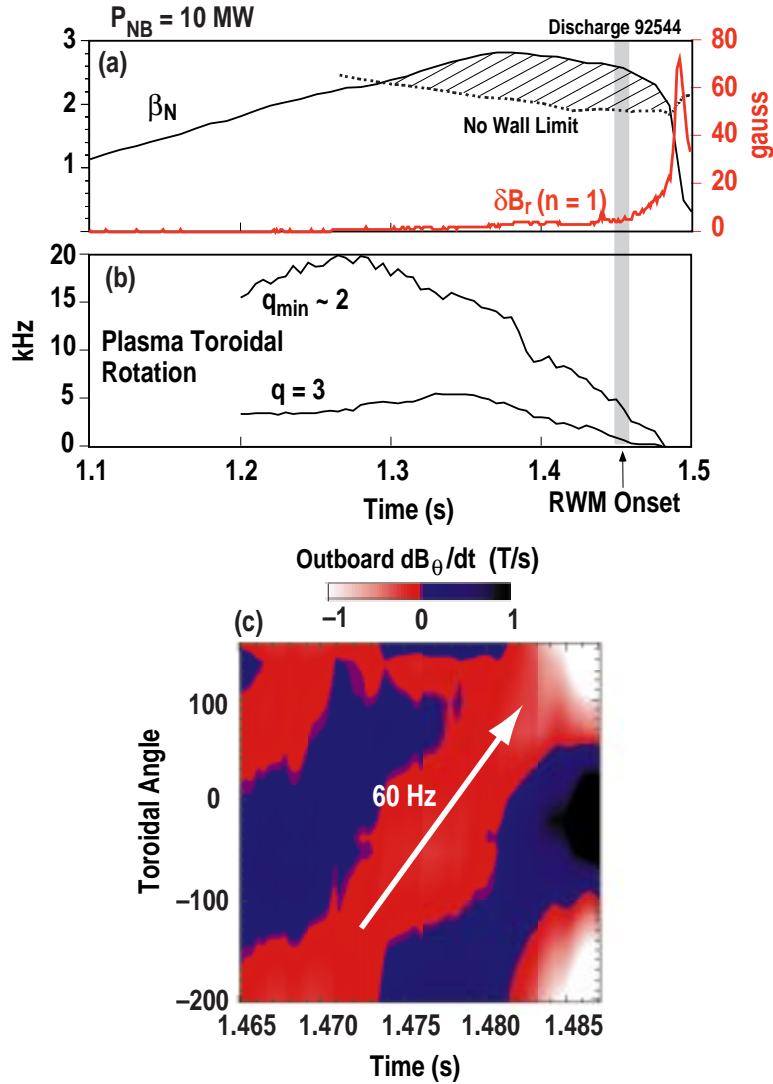


Fig. 9. Resistive wall mode stabilized by plasma rotation; (a) normalized beta, experimental solid curve, calculated ideal limite with no wall, dotted cureve; (b) plasma rotation measured by charge exchange recombination; (c) mode amplitude shown in toroidal angel vs. time, indicating mode rotation.

near the $q = 3$ surface falls below approximately 1 kHz, Fig. 9(b). The unstable mode grows with a much slower rotation frequency than the plasma rotation frequency [Fig. 9(c)]. In some cases the critical plasma rotation frequency is ~ 6 kHz, while the mode rotation frequency remains very slow, < 60 Hz. The growth rate of the mode for this case is approximately $(8 \text{ ms})^{-1}$, approximately the inverse wall time, as predicted by theory.^{31,32}

Active means of avoiding the RWM are being pursued by controlling either the plasma rotation or the RWM directly. As is shown in Fig. 10, preliminary results from open loop RWM control experiments have demonstrated that the RWM is suppressed by

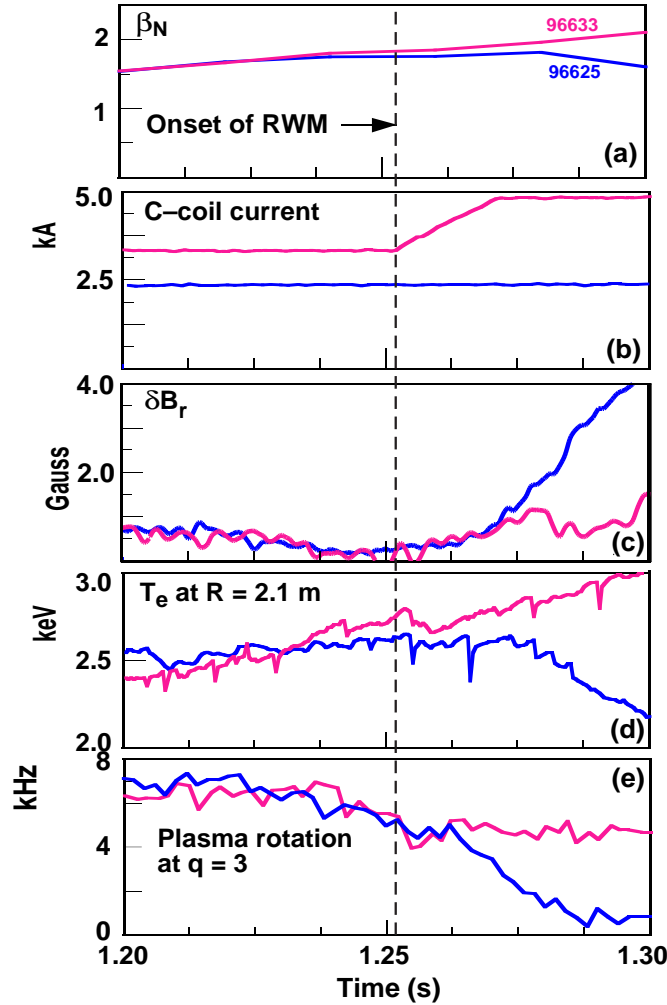


Fig. 10. Time history of discharges with (96633) and without (96625) pro-active control of the RWM (a) β_N , (b) current in the C-coil, (c) perturbed radial field measured on the saddle loops, (d) ECE measurement of the electron temperature at $R = 2.1$ M, (e) plasma rotation at the $q=3$ surface. Note that the perturbed radial field grows without bound in the case with constant C-coil current but is stabilized by stepping up the C-coil current with the proper toroidal phase.

the application of an appropriate correction field using an external coil set located far outside the plasma. A series of discharges with reproducible RWM onset were run, but one discharge used an $n = 1$ (C-coil) perturbation which was proactively programmed to turn on at the time of the RWM onset with a phase opposing the mode (Fig. 10). As observed from plasma rotation and T_e profiles near $q = 3$, the RWM started to grow but was suppressed and the plasma recovered when the opposing field was applied. The $n=1$ radial field soaking through the vacuum vessel wall was measured by a saddle loop array. As is shown in Fig. 10, this field grows without bound in the reference shot without the external $n=1$ field but remains at a low level with the external field applied, indicating

that control was achieved. New experiments in DIII-D with new active feedback power supplies are planned next year to pursue this further.

Another factor in obtaining steady-state improved performance discharges is control of edge transport and stability. Both theoretical expectations^{34,35} and the DIII-D results indicate a connection between the edge pressure pedestal height and the overall energy confinement.³⁶ In addition, edge stability affects ELM frequency and amplitude, which have a major impact both on core transport barriers and on the divertor. Although there has been considerable speculation that the edge pressure gradient just before an ELM is limited by high-n ballooning, detailed measurements on DIII-D have shown that the pressure gradient exceeds this limit by at least a factor of two.³⁶ The bootstrap current, driven by the large edge pressure gradient, opens up a ballooning second stable region at the plasma edge. Accordingly, the edge pressure is not limited by high-n ballooning but rather by other, lower n MHD modes which are driven unstable by the large pressure and current gradients that ballooning stability allows.^{29,37,38} Modes with toroidal mode numbers $3 < n < 5$ have are calculated ideal unstable by the GATO code. It is conjectured that these lower n instabilities couple more effectively to the core at high beta, making it more difficult to develop an ITB with large ELMs.

V. DIVERTOR PHYSICS AND THE DENSITY LIMIT

A tokamak density limit scaling of the form $n_e \propto I_p/a^2$ has been reported by several authors^{39,40} where I_p is the plasma current and a is the minor radius. However, extrapolation of this scaling to reactors can be misleading because the underlying physical processes have not been determined. We have conducted a series of experiments on DIII-D to determine the density-limiting processes in tokamaks.^{41,42} Using the understanding gained through these experiments, we have succeeded in obtaining high confinement plasmas at densities above the limit of the Hugill-Greenwald scaling.^{42,43} A key result of these studies is that the $n=0$, $m=1$ MARFE condensation instability criterion⁴⁴ is in quantitative agreement with high resolution edge measurements on DIII-D.⁴⁵ Additionally, we have shown that the MARFE instability condition combined with ITER89P confinement scaling yields an edge density limit scaling of the form:

$$n_e^{\text{crit}} \propto \frac{I_p^{0.96}}{a^{1.9}} \xi^{-0.11} P_{\text{heat}}^{0.43} R^{0.17} B_T^{0.04} [\kappa^2(1+\kappa^2)]^{-0.22},$$

where ξ_i is the impurity concentration and κ is the plasma elongation. Except for a moderate power dependence this scaling is remarkably similar to the Hugill-Greenwald scaling. The insensitivity to all plasma parameters except I_p and minor radius a derives from the fact that the MARFE density threshold for low Z impurities (e.g. oxygen or carbon) for an electron temperature range of 10–100 eV increases with the fourth power of T_e . Accordingly, a MARFE nearly always occurs at the same boundary temperature (~ 20 eV). Therefore, the trade off between density and temperature in the stored energy determines the density scaling. Thus, we conclude that future devices with high fusion power producing high edge temperatures should access densities well above the nominal Hugill-Greenwald limit.

Experiments on DIII-D have obtained high density discharges, $n_e/n_G \sim 1$, with good H-mode confinement, by a technique employing strong deuterium puffing, impurity Argon puffing and at the same time, strong pumping in the divertor.⁴⁶ As can be seen in Fig. 11, energy confinement remains high during the argon injection. For this discharge, $n_e/n_G \sim 0.75$. These are partially detached discharges, and the strong pumping is required to maintain thermal stability of the plasma edge. Note in Fig. 11(b), that the electron pressure pedestal does not significantly decrease during the argon injection. In

Fig. 11(c), and 11(d) are shown the energy confinement time as the total radiated power fraction increases toward unity and n_e/n_G approaches unity: no significant decrease in the confinement enhancement is noted. These results indicate high confinement at high density is possible, and suggest further research of the density limiting mechanism.

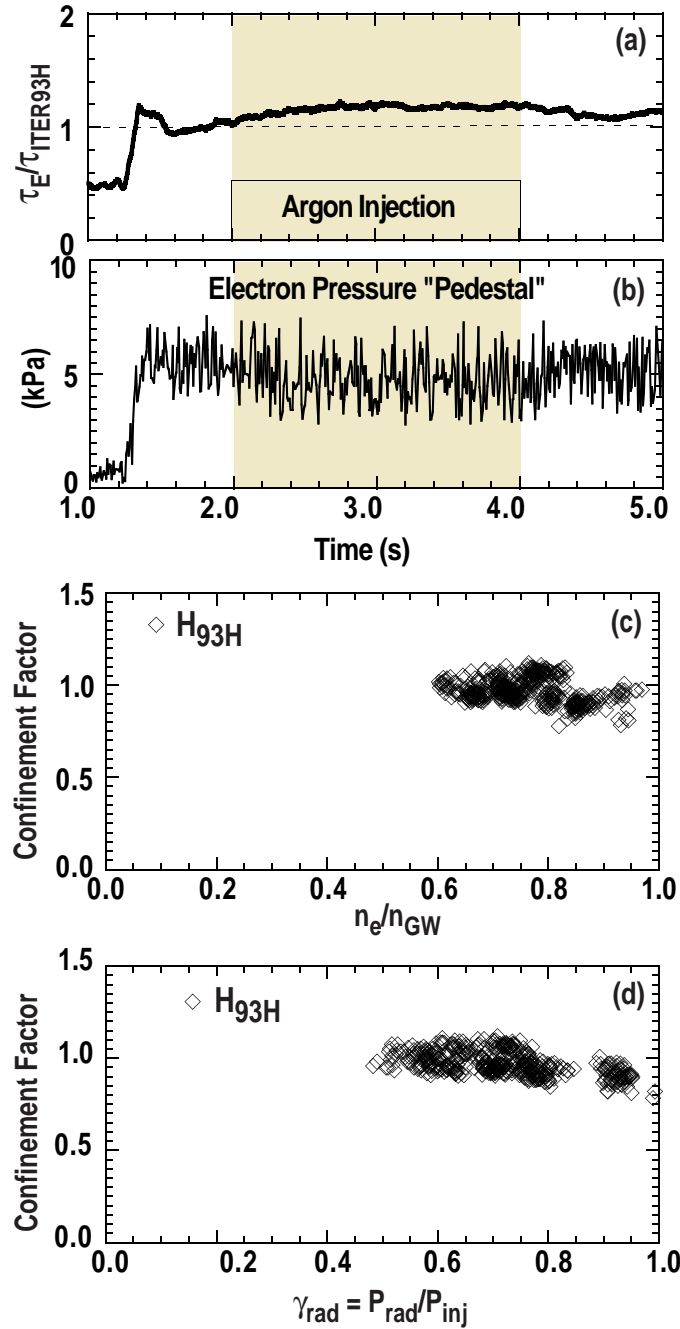


Fig. 11. Energy confinement at high density; (a) temporal evolution of confinement enhancement and argon injection; (b) temporal evolution of electron pedestal pressure, (c) confinement enhancement vs. radiation fraction, (d) confinement enhancement vs. n_e/n_G .

Through experiments on DIII-D⁴⁷⁻⁵⁰ we have demonstrated the efficacy of using induced scrape-off-layer (SOL) flows to preferentially enrich impurities in the divertor plasma. These SOL flows are produced through simultaneous deuterium gas injection at the midplane and divertor exhaust using cryopumping. Using this SOL flow, an improvement in enrichment (defined as the ratio of impurity fraction in the divertor to that in the plasma core) has been observed for all impurities in trace-level experiments (i.e., impurity level is non-perturbative), with the degree of improvement increasing with impurity atomic number. In the case of argon, exhaust gas enrichment using a modest SOL flow is as high as 17. Using this induced SOL flow technique and argon injection, radiative plasmas have been produced that combine high radiation losses ($P_{\text{rad}}/P_{\text{input}} > 70\%$), low core fuel dilution ($Z_{\text{eff}} < 1.9$), and good core confinement ($\tau_E \gtrsim \tau_{E,\text{ITER98Hy}}$).

DIII-D measurements clearly indicate that convection plays a dominant role in the heat particle transport in detached plasmas. Parallel thermal conduction based on measured divertor density and temperature profiles in detached plasmas is too small to account for the divertor heat flux. A one-dimensional interpretive model of the detached divertor plasma⁵¹ has been developed for further understanding of the experimental observations. The model calculates the parallel heat flux in the divertor plasma by integrating plasma radiation, obtained from an inversion of the bolometer data, from the target to a point in the divertor plasma and using the target heat flux, measured by an IR camera, as the boundary condition. The difference between this heat flux and the conduction heat flux, obtained from the measured T_e profile, yields the convective component of the heat flux. It is found that in attached plasmas, with measured electron temperatures of approximately 20 eV just in front of the plate, the conduction component accounts for nearly all the heat flux. In contrast, in the detached case, with electron temperatures 1–2 eV near the divertor plate, the conduction channel is insignificant compared to the total heat flux and convection at approximately the sound speed is required to account for most of the heat flux.

Experimental results and UEDGE modeling⁵² indicate a broad regions of Mach ~ 0.4 flow and copious volume recombination near the target plate in detached plasmas (Fig. 12). Visible and UV line ratio measurements^{53,54} show direct evidence of volume recombination [Fig. 12(b)]. Plasma parallel flow speeds at or near the sound speed are also observed by spectroscopy [Fig. 12(c)]⁵³ as well as a Mach probe.⁵⁵ From Langmuir probe potential measurement,⁵⁶ we also deduce poloidal $E_r \times B_T$ flows. The flow direction depends on the direction of the toroidal field and heat and particle flux associated with it is estimated to contribute significantly to particle exchange between the two divertor strike points and could explain the field-dependent divertor in-out asymmetry.

We have recently installed a divertor baffle and cryopump⁵⁶ at the upper divertor whose shape is matched for particle control in high triangularity plasmas ($\delta \sim 0.7$).

Measurements and UEDGE and DEGAS calculations indicate a decrease in core ionization of a factor ~ 2.5 for the baffled divertor discharge compared otherwise similar unbaffled discharges. With the upper cryopump turned on, we achieved active density control with $n_e/n_{Gr} = 0.27$, which is similar to the 0.22 achieved with the lower pump. This establishes an important particle control tool for high triangularity plasma operation in DIII-D. In 1999, we will install a third divertor cryopump for the purpose of pumping the inner strike point in the upper divertor.⁵⁶ In addition, a structure in the private flux region which protects the inner pump will serve also as a baffle to further reduce core ionization an additional factor of 2 and isolate the two strike points.

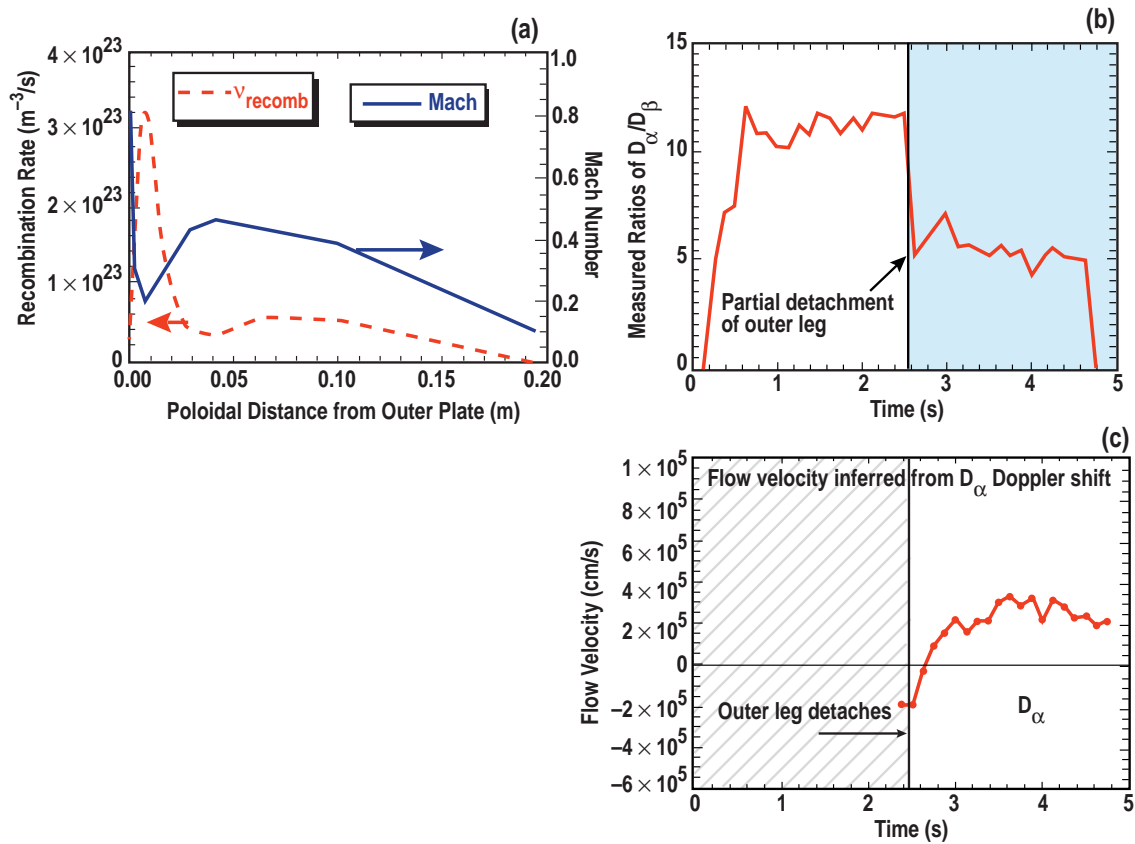


Fig. 12. (a) Modeling of a partially detached plasma shows Mach 0.4 flow in the bulk of the divertor plasma and copious volume recombination near the target plate. (b) D_{α}/D_{β} line ratio indicate recombination after detachment. (c) Flow speed of the order of 1/4 sound speed is measured by spectroscopy.

VI. SUMMARY

The research program on DIII-D is aimed at developing the scientific basis for advanced modes of operation which have the potential of enhancing the commercial attractiveness of a the tokamak as an energy producing system. We have demonstrated integrated, high performance ELMing H-mode plasmas with $\beta_N H_{89P} \sim 10$ ($\beta_N H_{98y} \sim 6$ for $5 \tau_E$ (~ 1 s)). We have shown that the core transport barrier can be sustained fully with steady profiles, limited only by the duration of the neutral injection, with no sign of deterioration of the barrier. The ion transport inside an ITB often reaches that predicted for neoclassical, but there is often little or no reduction in the electron transport. An ITB in the electron thermal transport is observed only in discharges with significant negative shear. Although the ion transport barrier continues to be well explained by sheared E×B flow stabilization of drift wave turbulence, drift wave turbulence together with E×B flow does not provide an explanation of electron transport. With the aim of current profile control in NCS discharges, we have demonstrated off-axis ECCD with an efficiency above theoretical predictions.

Experiments and theory have shown the sensitivity of the beta limit on the pressure profile, indicating the advantage of broad pressure profiles in shaped discharges. The stability limit against neoclassical tearing modes has been increased in long pulse discharges, by keeping $q(0) > 1$, avoiding sawteeth and eliminating the seed islands. Discharges with beta significantly above the ideal no wall limit have been reproducibly obtained showing clear evidence of stabilization of the resistive wall mode by plasma rotation. Initial experiments with non-axisymmetric coils have delayed the onset of the RWM and are promising for future planned active feedback experiments.

We have developed and tested a model of the density limit which agrees with the Hugill-Greenwald scaling and which scales favorably to larger hotter devices. In DIII-D, discharges with deuterium and argon puffing together with strong divertor pumping approach the Greenwald density limit with little or no deterioration in confinement. Strong edge plasma flows have also been used to increase the edge and divertor radiation and increase the divertor enrichment. The DIII-D experiments have measured divertor electron temperatures of 1–2 eV, which together with the measured heat flow clearly indicate the role of convection in heat and particle flow. The predicted Mach level flows and recombination radiation have been measured.

The DIII-D future research continues to remain focused on the optimization of the tokamak. On a three year time scale, we are aiming at an integrated demonstration of

advanced tokamak operation sustained for five seconds. Important new control tools will include an upper private flux baffle with a cryopump, an increase in ECCD power to a 6 MW system, and an 18 coil set for active feedback of the resistive wall mod. In the nearer term, our experiments will emphasize expanding the spatial extent of internal transport barriers, regulating edge bootstrap currents, stabilizing neoclassical tearing modes, feedback stabilizing high-beta resistive wall modes, and developing the basis for radiative divertors in both single and double null configurations.

REFERENCES

- ¹ITER Physics Basis Document, Nuclear Fusion (to be published). JET report JET-P(98)-17.
- ²P.N. Yushmanov, Nucl. Fusion **30**, 1999 (1990).
- ³T.S. Taylor, Plasma Phys. Control. Fusion **39**, B47 (1997).
- ⁴J.D. Galambos, et al., Nucl. Fusion **35**, 551 (1995).
- ⁵S.C. Jardin, et al., Fusion Eng. Design **38**, 27 (1997).
- ⁶B.W. Rice, et al., Proc. of the 17th IAEA Fusion Energy Conf., Yokohama, Japan 1998 (International Atomic Energy Agency, to be published in special issue of Nucl. Fusion).
- ⁷E.J. Strait, et al., Phys. Rev. Lett. **75**, 4421 (1995).
- ⁸B.W. Rice, Phys. Plasmas **3**, 1983 (1996).
- ⁹F.X. Söldner, et al., Plasma Phys. Control. Fusion **39**, B353 (1997).
- ¹⁰Y. Koide, et al., Phys. Plasmas **4**, 1623 (1997).
- ¹¹F.M. Levinton, et al., Phys. Rev. Lett. **75**, 4417 (1995).
- ¹²E.J. Synakowski, et al., Phys. Plasmas **4**, 1736 (1997).
- ¹³T. Ozeki, et al., Nucl. Fusion **33**, 1025 (1993).
- ¹⁴C. Kessel, Phys. Rev. Lett. **72**, 1212 (1994).
- ¹⁵J. Manickam, Phys. Plasmas **1**, 1601 (1994).
- ¹⁶A.D. Turnbull, et al., Phys. Rev. Lett. **74**, 718 (1995).
- ¹⁷E.A. Lazarus, et al., Phys. Rev. Lett. **77**, 2714 (1996).
- ¹⁸T. Fujita, et al., Phys. Rev. Lett. **78**, 2377 (1997).
- ¹⁹K.H. Burrell, Phys. Plasmas **4**, 1499 (1997).
- ²⁰B.W. Stallard, et al., "Electron Heat Transport in Improved Confinement Discharges in DIII-D," to be published in Phys. Plasmas and General Atomics Report GA-A23020.
- ²¹G.M. Staebler, et al., Proc. of the 17th IAEA Fusion Energy Conf., Yokohama, Japan 1998 (International Atomic Energy Agency, to be published in special issue of Nucl. Fusion).
- ²²E.J. Synakowski, Proc. of the 17th IAEA Fusion Energy Conf., Yokohama, Japan 1998 (International Atomic Energy Agency, to be published in special issue of Nucl. Fusion).
- ²³K.H. Burrell, et al., Plasma Phys. Control. Fusion **40**, 1585 (1998).
- ²⁴C.M. Greenfield, Proc. of the 17th IAEA Fusion Energy Conf., Yokohama, Japan 1998 (International Atomic Energy Agency, to be published in special issue of Nucl. Fusion).
- ²⁵C.L. Rettig, et al., Phys. Plasmas **5**, 1727 (1998).
- ²⁶T.C. Luce, et al., Proc. of the 17th IAEA Fusion Energy Conf., Yokohama, Japan 1998 (International Atomic Energy Agency, to be published in special issue of Nucl. Fusion).
- ²⁷C.B. Forest, et al., Phys. Rev. Lett. **73**, 2244 (1994).

- ²⁸A.D. Turnbull, et al. "Synergism Between Cross-Section Shaping and Profile Shaping in Beta Optimization of Tokamak Equilibria With Negative Central Shear," to be published in Nucl. Fusion (1998).
- ²⁹E.J. Strait, et al., Phys. Plasmas **4**, 1783 (1997).
- ³⁰R.J. La Haye, et al., Plasma Phys. and Contr. Nucl. Fusion Research 1996 (International Atomic Energy Agency, Vienna, 1997), Vol. 1, p. 747.
- ³¹A.M. Garofalo, et al., "Direct Observation of the Resistive Wall Mode in a Tokamak and Its Interaction With Plasma Rotation," General Atomics Report GA-A22985 (1998), submitted to Phys. Rev. Lett.
- ³²E.J. Strait, et al., Proc. of the 17th IAEA Fusion Energy Conf., Yokohama, Japan 1998 (International Atomic Energy Agency, to be published in special issue of Nucl. Fusion).
- ³³A.M. Garofalo, et al., "Stabilization of the External Kink and Control of the Resistive Wall Mode in Tokamaks," to be published in Phys. Plasmas.
- ³⁴M. Kotschenreuter, et al., Plasma Phys. and Contr. Nucl. Fusion Research 1996 (International Atomic Energy Agency, Vienna, 1997) Vol. 2, p. 371.
- ³⁵R.E. Waltz, et al., Plasma Phys. and Contr. Nucl. Fusion Research 1996 (International Atomic Energy Agency, Vienna, 1997) Vol 2, p. 385.
- ³⁶T.H. Osborne, et al., Proc. of the 13th Intl Conf. on Plasma Surface Interactions, San Diego, California, 1998, to be published in J. Nucl. Mater.
- ³⁷L.L. Lao, et al., Proc. of the 17th IAEA Fusion Energy Conf., Yokohama, Japan 1998 (International Atomic Energy Agency, to be published in special issue of Nucl. Fusion).
- ³⁸E.J. Strait, et al., Contr. Fusion and Plasma Physics (Proc. 20th Euro. Conf. on Contr. Fusion and Plasma Physics, Lisbon 1993) (European Physical Society, Petit Lancy, 1994) Vol. 1, p. 211.
- ³⁹J. Hugill, et al., Heating in Toroidal Plasmas (Proc. 2nd Joint Varenna-Grenoble Int. Symp., Como, 1980), Vol. 2, CEC, Brussels (1980) 775.
- ⁴⁰M. Greenwald, et al., Nucl. Fusion **2**, 2199 (1988).
- ⁴¹M.A. Mahdavi, et al., Plasma Phys. and Contr. Nucl. Fusion Research 1996 (International Atomic Energy Agency, Vienna, 1997), Vol 1, p. 397.
- ⁴²R. Maingi, et al., Proc. of the 17th IAEA Fusion Energy Conf., Yokohama, Japan 1998 (International Atomic Energy Agency, to be published in special issue of Nucl. Fusion).
- ⁴³R. Maingi, et al., Phys. Plasmas **4**, 1752 (1997).
- ⁴⁴J.F. Drake, Phys. Fluids **30**, 8 (1987).
- ⁴⁵M.A. Mahdavi, et al., Contr. Fusion and Plasma Phys. (Proc. 24th Euro. Conf. on Contr. Fusion and Plasma Physics, Berchtesgaden, 1997) (EPS Petit Lancy, 1997) Vol. 3, p. 1113
- ⁴⁶G.L. Jackson, et al., Proc. of the 13th Int. Conf. on Plasma Surface Interactions, San Diego, California, 1998, to be published.
- ⁴⁷M.J. Schaffer, et al., Nucl. Fusion **8**, 1000 (1995).
- ⁴⁸M.J. Schaffer, et al., J. Nucl. Mater. **241-243**, 585 (1997).

- ⁴⁹M.R. Wade, et al., "Impurity Enrichment Studies with Induced Scrape-Off Layer Flow," to be published in Nucl. Fusion (1998).
- ⁵⁰M.R. Wade, et al., "Impurity Entrainment Studies Using Induced SOL Flow in DIII-D," Proc. of the 13th Inter. Conf. on Plasma Surface Interactions in Contr. Fusion Devices, San Diego, California, 1998, to be published in J. Nucl. Mater.
- ⁵¹A.W. Leonard, et al., Phys. Rev. Lett. **78**, 4769 (1997).
- ⁵²G.D. Porter, et al., Phys. Plasmas **3**, 1967 (1997).
- ⁵³R.C. Isler, et al., Proc. of the 13th Inter. Conf. on Plasma Surface Interactions in Contr. Fusion Devices, San Diego, California, 1998, to be published in J. Nucl. Mater.
- ⁵⁴M.E. Fenstermacher, et al., "Physics of the Detached Radiative Divertor Regime in DIII-D," Proc. of the 25th EPS Conf. on Contr. Fusion and Plasma Phys., Prague, Czech Republic, 1998, to be published.
- ⁵⁵J.A. Boedo, et al., "Plasma Flow in the DIII-D Divertor," Proc. of the 25th EPS Conf. on Contr. Fusion and Plasma Phys., Prague, Czech Republic, 1998, to be published.
- ⁵⁶S.L. Allen, et al., "Studies of Baffled and Open Pumped Divertor Operation on DIII-D," Proc. of the 13th Inter. Conf. on Plasma Surface Interactions in Contr. Fusion Devices, San Diego, California, 1998, to be published in J. Nucl. Mater.

ACKNOWLEDGMENTS

This is a report of work supported by the U.S. Department of Energy under Contract Nos. DE-AC03-99ER54463, DE-AC05-96OR22464, DE-AC02-76CH03073, W-7405-ENG-48, and Grant No. DE-FG03-96ER54373. The author would like to acknowledge the many contributions from the entire DIII-D Team in the research presented herein.

DIII-D TEAM

S.L. Allen,^{a)} P.M. Anderson,^{b)} M.E. Austin,^{c)} D.S. Baggert,^{b)} W. Baity,^{d)} D.R. Baker,^{b)} D.E. Baldwin,^{b)} G. Barber,^{d)} R. Bastasz,^{e)} C.B. Baxi,^{b)} L. Baylor,^{d)} S. Bernabei,^{f)} J. Bialek,^{g)} J.A. Boedo,^{h)} A. Bondeson,ⁱ⁾ A.S. Bozek,^{b)} R. Bravenec,^{c)} B.D. Bray, J.D. Broesch,^{b)} N.H. Brooks,^{b)} K.H. Burrell,^{b)} J. Callen,^{j)} R.W. Callis,^{b)} C.S. Campo,^{b)} T.N. Carlstrom,^{b)} E. Carolipio,^{k)} B. Carreras,^{d)} W.P. Cary,^{b)} T.A. Casper, V.S. Chan,^{b)} M. Chance,^{f)} L. Chen,^{l)} E. Chin,^{b)} H.K. Chiu,^{b)} M. Chu,^{b)} R.J. Colchin,^{d)} S. Combs,^{d)} J.W. Cuthbertson,^{h)} W. Davis,^{f)} J.C. De Boo,^{b)} J.S. deGrassie,^{b)} R. Deranian,^{m)} G. Diao,ⁿ⁾ J.L. Doane,^{b)} E.J. Doyle,^{o)} R. Ellis,^{p)} T.E. Evans,^{b)} M.E. Fenstermacher,^{a)} J.R. Ferron,^{b)} D. Finkenthal,^{q)} R. Fonck,^{j)} E. Fredrickson,^{f)} J. Freeman,^{b)} R.L. Freeman,^{b)} J. Gafert,^{r)} S. Galkin,^{s)} A. Garofalo,^{g)} G. Garstka,^{p)} G. Giruzzi,^{t)} P. Gohil,^{b)} A.A. Gootgeld,^{b)} F. Grantham,^{b)} D. Gray,^{h)} J.M. Greene,^{b)} K.L. Greene,^{b)} C.M. Greenfield,^{b)} N. Greenough,^{f)} R.J. Groebner,^{b)} S. Guenter, M.J. Hansink,^{b)} T.E. Harris,^{b)} R.W. Harvey,^{u)} T. Hatae,^{v)} C. Hegna,^{j)} W.W. Heidbrink,^{k)} D.N. Hill,^{a)} F.L. Hinton,^{b)} E.H. Hoffmann,^{b)} J. Hogan,^{d)} K.L. Holtrop,^{b)} R.-M. Hong,^{b)} W. Houlberg,^{d)} C.L. Hsieh,^{b)} D.A. Humphreys,^{b)} A.W. Hyatt,^{b)} H. Ikezi,^{b)} R.C. Isler,^{d)} G.L. Jackson,^{b)} N. Jaluka,^{w)} T.H. Jensen,^{b)} T. Jernigan,^{d)} R.D. Johnson,^{b)} L. Johnson,^{f)} D.H. Kaplan,^{b)} K.M. Keith,^{b)} A.G. Kellman,^{b)} D.H. Kellman,^{b)} R. Khayrutdinov,^{x)} J.F. Kinsey,^{y)} R.J. La Haye,^{b)} G. Labik,^{f)} L.L. Lao,^{b)} C.J. Lasnier,^{a)} E.A. Lazarus,^{d)} R.L. Lee,^{b)} J. Lee,^{h)} R.A. Legg,^{b)} R. Lehmer,^{h)} A.W. Leonard,^{b)} J.A. Leuer,^{b)} Y.R. Lin-Liu,^{b)} J.M. Lohr,^{b)} T.C. Luce,^{b)} S. Luckhardt,^{h)} V. Lukash,^{x)} J. Luo,^{l)} J.L. Luxon,^{b)} M.A. Mahdavi,^{b)} R. Maingi,^{d)} C.C. Makariou,^{b)} J. Mandrekas, B.B. McHarg Jr.,^{b)} G.E. McKee,^{j)} W.H. Meyer,^{a)} K.R. Mittlehaug,^{b)} R.L. Miller,^{b)} P.K. Mioduszewski,^{d)} J. Moller,^{a)} R.A. Moyer,^{h)} M. Murakami,^{d)} A. Nagy,^{f)} G.A. Navratil,^{g)} A. Nerem,^{b)} W. Nevins,^{a)} D.E. Nilson,^{a)} L.E. Nissley,^{b)} R.C. O'Neill,^{b)} T.H. Osborne,^{b)} L. Owens,^{d)} P.B. Parks,^{b)} R. Parsell,^{f)} A.W. Peebles,^{o)} B.G. Penaflo,^{b)} Q. Peng,^{b)} R. Perkins,^{f)} P.I. Petersen,^{b)} T.W. Petrie,^{b)} C.C. Petty,^{b)} J.C. Phillips,^{b)} D.A. Piglowski,^{b)} R.I. Pinsker,^{b)} P.A. Politzer,^{b)} D. Ponce,^{b)} G.D. Porter,^{a)} R. Prater,^{b)} S.G. Pronko,^{b)} A. Punjabi,^{w)} A. Ramsey,^{f)} E.E. Reis, Jr.,^{b)} D.E. Reimsen,^{b)} C. Ren,^{j)} M.E. Rensink,^{a)} C.L. Rettig,^{o)} T.H. Rhodes,^{o)} B.W. Rice,^{a)} J.I. Robinson,^{b)} D. Ross,^{c)} C. Rost,^{aa)} S. Sabbagh,^{g)} S. Sakurai,^{v)} R.I. Savercool,^{b)} J.M. Schachter,^{b)} M.J. Schaffer,^{b)} D.P. Schissel,^{b)} J.T. Scoville,^{b)} D.L. Sevier,^{b)} T.C. Simonen,^{b)} S.M. Skinner,^{b)} J.P. Smith,^{b)} R.T. Snider,^{b)} H.E. St John,^{b)} W. Stacey,^{z)} G.M. Staebler,^{b)} B.W. Stallard,^{a)} R.D. Stambaugh,^{b)} E.J. Strait,^{b)} E. Synakowski,^{f)} P.L. Taylor,^{b)} T.S. Taylor,^{b)} T. Terpstra,^{f)} D.M. Thomas,^{b)} S. Turgarinov,^{x)} A.D. Turnbull,^{b)} R. Vernon,^{j)} M.R. Wade,^{d)} M.I. Walker,^{b)} R.E. Waltz,^{b)} W.R. Wampler,^{e)} Z. Wang,ⁿ⁾ A.M. Warner,^{b)} J.G. Watkins,^{e)} W.P. West,^{b)} J. Whaley, Jr.,^{e)} D.G. Whyte,^{h)} H. Wilson,^{bb)} N. Wolf,^{a)} R. Wolf,^{r)} C.P.C. Wong,^{b)} K. Wong,^{f)} F. Yin,^{l)} L. Zeng,^{o)} M. Zerbini,^{cc)} C. Zhang^{d)}

^{a)}Lawrence Livermore National Laboratory,
Livermore, CA.

^{b)}General Atomics, San Diego, CA.

^{c)}University of Texas at Austin, Austin, TX.

^{d)}Oak Ridge National Laboratory, Oak Ridge, TN.

^{e)}Sandia National Laboratories, Livermore, CA.

^{f)}Princeton Plasma Physics Laboratory, Princeton,
NJ.

^{g)}Columbia University, New York, NY.

^{h)}University of California, San Diego, La Jolla, CA.

ⁱ⁾Chalmers University, Götteborg, Sweden.

^{j)}University of Wisconsin, Madison, WI.

^{k)}University of California, Irvine, CA.

^{l)}ASIPP, Hefei, Peoples Republic of China.

^{m)}University of Wales.

ⁿ⁾Southwest Institute, China.

^{o)}University of California, Los Angeles, CA.

^{p)}University of Maryland, College Park, MD.

^{q)}Palomar College, San Marcos, CA.

^{r)}IPP, Garching, Germany.

^{s)}Keldysh Institute, Moscow, Russia

^{t)}Assoc.-EURATOM-CEA, Cadarache, France.

^{u)}Comp-X, Del Mar, CA

^{v)}Japan Atomic Energy Research Institute, Naka,
Japan

^{w)}Hampton University, Hampton, VA.

^{x)}TRINITI, Troitsk, Russia.

^{y)}LeHIGH University, Bethlehem, PA

^{z)}Georgia Tech, Atlanta, GA

^{aa)}MIT, Cambridge, MA.

^{bb)}Culham, Abingdon, UK.

^{cc)}ANEA, Frascati, Italy.